Applied Thermal Engineering 180 (2020) 115923

Contents lists available at ScienceDirect

Applied Thermal Engineering

journal homepage: www.elsevier.com/locate/apthermeng

Performance assessment of a heat pump and a concentrated photovoltaic thermal system during the wood drying process

Ahmed Khouya

Department of Electrical and Industrial Engineering, National School for Applied Sciences, Abdelmalek Essaâdi University, B.P. 1818 Tangier, Morocco

HIGHLIGHTS

- A new water/air heat pump is proposed for carrying out the drying.
- A new mathematical model for concentrated photovoltaic thermal is proposed.
- A hybrid solar dryer suitable for softwood drying is proposed.
- High performance hybrid dryer compared to that presented in the literature.

ARTICLE INFO

Keywords:
Heat pump
Concentrated photovoltaic thermal
Energy consumption
Drying capacity
Performance

ABSTRACT

Wood drying is an unavoidable step to bring to the market products with higher added value. Achieving drying under certain economic conditions requires calculating the drying cost with great precision while minimizing energy consumption. Conventional dryers with very high heating power are useful, but their energy consumption and greenhouse gas emissions remain too high. This work aims to propose a water/air heat pump powered by a concentrated photovoltaic thermal as a new hybrid solution for carrying out the drying process of softwood. The drying system consists of four main units, a drying chamber, a Closed Feed Air Heater, a water/air heat pump and a concentrated photovoltaic thermal. The study is based on the establishment of energy and mass balances in the drying system. The governing equations of the drying model are solved using the finite difference method. A perfect agreement is obtained between experimental and numerical results. The results show that the electrical energy consumption ratio using a heat pump as the main heater device fluctuates between 29 and 52 $kWh.m^{-3}$. The coefficient of performance also ranges from 3.91 to 7.2. The results show that a decrease of the heat pump set temperature from 75 to 65 °C improves the coefficient of performance at least 17%. The combined use of heat pump and concentrated photovoltaic thermal system has the effect of reducing the energy consumption ratio up to 86%. The effect of parameters such as optical efficiency, concentration ratio and evaporator air temperature on drying performance is investigated. The results show that the heat recovered at the Closed Feed Air Heater increases as the temperature of air leaving the dryer increases. A decrease in optical efficiency from 0.9 to 0.65 increases the electrical energy consumption ratio by 73%. An increase in the aperture area from 100 to 150 m^2 also improves electricity production and drying capacity by 45 and 27%, respectively. The drying capacity has known an increase of about 43% by increasing the mass flow rate from 0.6 to 1 $kg.s^{-1}$. Finally, the combined use of a heat pump and a concentrated photovoltaic thermal can reduce significantly the electrical energy consumption and improve thermal performance of drying systems throughout the year.

1. Introduction

Drying in most industrial units is carried out by relatively powerful fuel and gas boilers which consume energy [1–3]. These heaters devices are highly polluting and responsible for the excessive emission of greenhouse gases having a harmful impact on the environment [4]. Therefore, it is necessary to integrate in the drying industry other heating appliances that consume less energy such as a heat pump, or to use solar kilns because they consume less electrical energy for their operation [5,6]. The advantages of solar dryers are the high quality of dried products, low acquisition and operating costs and they are simple to mount and manage their operation. Nevertheless, their disadvantage is that they are intermittent compared to conventional dryers and depend on weather conditions. Today with the globalization of markets, especially those of the wood drying industry, the engineer is obliged to produce high quality dried wood quickly at a lower cost. The best drying strategy is one that, for a given species, optimally meets the requirements of rapidity, quality and cost. Timber drying is also an economic necessity as it meets the increasingly stringent requirements of consumers, helps to increase the added value of the product and

https://doi.org/10.1016/j.applthermaleng.2020.115923
Received 25 April 2020; Received in revised form 2 August 2020; Accepted 13 August 2020
Available online 18 August 2020
1359-4311/

Nomenclature

Symbols

A	Exchange area (m^2)
A_c	Collector area (m^2)
C_p	Specific heat ($kJ.kg^{-1}.K^{-1}$)
Cr	Concentration ratio (-)
D_a	Water vapor diffusion coefficient ($m^2.s^{-1}$)
D_w	Mass diffusion coefficient ($m^2.s^{-1}$)
e	Thickness (m)
K	Conductive heat transfer coefficient ($W.m^{-2}.K^{-1}$)
Kg	Overall mass transfer coefficient ($kg.m^{-2}.s^{-1}$)
h	Heat coefficient transfer ($W.m^{-2}.K^{-1}$)
L_c	Collector Length (m)
m	Mass (kg)
M	Mass of wood (kg)
$\dot{m}_a$	Mass flow rate ($kg.s^{-1}$)
N	Number of wood segments
RH	Relative humidity (-)
S	Surface (m^2)
t	Time (s)
T	Temperature (K)
u	Air velocity ($m.s^{-1}$)
V	Volume (m^3)
W	Absolute humidity (kg water/kg dry air)
X	Moisture content (kg water/ kg dry matter)

Greek letters

ΔH	Latent heat ($kJ.kg^{-1}$)
ΔP	Pressure drop (Pa)
Δt	Time step (s)
ε	Emissivity (-)
η	Efficiency (-)
λ	Thermal conductivity of air ($W.m^{-1}.K^{-1}$)
μ	Effective permeability (-)
σ	Stefan-Boltzmann constant (5.67×10^{-8} $W.m^2.K^{-4}$)
ρ	Density ($kg.m^{-3}$)

Subscripts

a	Air
AC	Actual
ae	Air exterior
aux	Auxiliaries
b	Board
c	convection
comp	Compressor
dr	Drying
eq	Equilibrium
ev	evoporator
ex	Exchanged heat
f	Fluid
fi	Final
i	Initial
in	Inlet
inv	Inverter efficiency
lay	Layer
mod	Module efficiency
oi	Oil
op	Optic
out	Outlet
pi	Pipe
pv	Photovoltaic
Ra	Return air
re	Reflector
rec	Receiver
s	Cross section
sat	Saturation
set	Ser-point
sky	Sky
th	Thermal
w	Water
wv	Water vapor

Abbreviation

COP	Coefficient of performance
CPV/T	Concentrated photovoltaic Thermal
ECR	Electrical energy consumption ratio
HEX	Heat exchanger
HTF	Heat transfer fluid
HP	Heat pump
MER	Moisture extraction rate
SMER	Specific moisture extraction rate

opens the door to international markets. Depending on the wood destination, it must have a reasonable humidity that allows a correct implementation during its exploitation, as well as good dimensional stability over time [7]. There are traditionally several wood drying techniques, among the most used, it was considered useful to mention: conventional drying, microwave drying, vacuum and outdoor drying. When drying process is carried out with technical means, it requires heat and energy in proportions that depend on the moisture content, the drying temperature, the specific characteristics of the product to be dried and the kiln design [8–10]. Therefore, it is necessary to use cleaner heating systems during drying which do not consume much energy such as a system combining a heat pump and a concentrated photovoltaic thermal system (CPV/T). This work will propose a combined heating system specially to carry out the drying operations of softwood. It will be an opportunity to present the innovation brought to a hybrid dryer operating on the basis of renewable energies. It is an environmentally friendly, applicable and less expensive solution.

The use of heat pumps for drying food products has recently attracted a lot of attention [11,12]. Heat pumps consume less electricity and generate more heat, allowing them to heat and cool an industrial process at a lower cost [13]. Szekeres and Jeswie [14] found that a heat pump consumes 12 to 68% less energy than conventional ovens operating at the same temperature. However, a major energy problem of heat pumps is the additional heating requirements for drying in cold climates [15]. A 13 m^3 forced air wood dryer equipped with a 5.6 kW HP running at lower temperature was experimentally studied under the Canadian climate [16]. Two drying experiments were conducted using electrical boiler integrated with HPs and Electrical heating coils. The initial water content was 29.1% for test 1 and 40.7% for test 2. The results showed that the drying time was 147.03 h for yellow birch and 240.67 h for hard maple. Using all-electrical drying test, the part of energy consumed by HPs was 30%, 62% for the backup coils and 8% for fans. The use of a hybrid drying system has resulted in a consumption of about 25% for HP, 66% for backup coils and 9% for fans. Recent advances in conventional heating techniques have made it possible to design efficient heat pumps compared to those marketed only a few years ago. Currently, there are three heat pump technologies: aerothermal HP, a geothermal HP and a hydrothermal HP. The coefficient of

performance (COP) is an indicator that measures the amount of electricity that could be consumed by a heat pump [17]. Which heat pump technology would have a better COP during the drying process? The COP of an air/air heat pump integrated with solar collector during the drying process of agricultural product in different dehumidification conditions ranged from 0.58 to 2.32 [18,19]. The COP of a water / air heat pump used for drying deserves to be examined in the literature. It was reported that a water/water heat pump used in geothermal energy has a better coefficient of performance, but its main disadvantage lies in the installation costs which are generally more expensive than those of an air/air HP [20]. However, with the new thermal regulation laws, federal and local incentives can significantly reduce the initial cost and allow HP owners to recover their investment in five to ten years [21]. Therefore, it is necessary to think of pairing these heat pumps with new energy sources such as solar energy and heat storage to reduce power consumption and quickly amortize the initial investment [22,23]. A shortage in the use of water/air heat pumps specially to conduct wood drying operations has been pointed out. In present work, the coefficient of performance for a water/air heat pump used for drying purpose will be evaluated for different climatic conditions. The effect of certain parameters such as the outside air temperature and the set point on drying performance will also be reviewed and analyzed.

As explained in the previous sections, the integration of renewable energies, in particular solar energy in hybrid dryers, can reduce the energy consumption of the conventional source and improve the thermal performance of production. So why not supply the water/air heat pump with green electricity and carry out the wood drying operations? Is it possible to produce the heat and electricity necessary for drying the wood from the same renewable source and improve the performance of the hybrid dryer? Among the means of producing electricity and heat are thermal photovoltaic concentrators and hybrid PV panels [24,25]. A concentrated photovoltaic thermal system (CPV/T) consists of at least five essential parts, a mirror, PV cells, a coolant plate, a pipe in which the Coolant circulates and a tracking system. This is a more promising technology, which could improve the efficiency of solar energy conversion systems, thereby ensuring the reduction of heat losses associated with the high operating temperature when used for heating applications. Several CPV/T performance surveys have been conducted over the past two decades [26–28]. A CPV/T system has been proposed to produce heat and electricity for industrial textile applications [29]. A numerical study about the CPV/T system equipped with a linear triangular receptor equipped with triple junction PV cells was performed [30]. The model makes it possible to locally assess the thermal and electrical parameters of the CPV/T system. Some works have been studied the performance of a hybrid CPV/T system capable of operating up to temperatures of 180 °C [31]. Thermal and electrical efficiencies are expected to be very high for most operating conditions. The effect of the solar flux profile on a CPV/T system efficiency was investigated [32]. Experiments have shown that the electrical efficiency of the system dropped from 15 to 9%, depending on the solar concentration ratio. Kandil et al., [33] carried out a study showing the effect of some physical and geometrical parameters on the performance of a CPV/T system under harsh climate, in Kuwait. The results showed that the temperature of PV cells increases with increasing concentration ratio and that the hybrid CPV/T system works effectively in a harsh hot climate. To the best knowledge of the author, it appears that the integration of CPV/T systems in wood drying applications is now a gap to be raised to enrich the literature. In present work, a CPV/T system will be proposed for possible use in industrial drying applications. The CPV/T system will be used to supply electricity to the water/air heat pump. Synthetic oil will be chosen as the coolant for PV cells and the thermal energy produced will be used to heat the drying air through the installation of an oil/air heat exchanger. This solution will considerably improve the thermal performance of the hybrid solar dryer compared to conventional systems which consume more energy and further pollute the atmosphere.

In the literature survey, there is a lack in determining thermodynamic parameters such as drying capacity, energy consumption and drying efficiency relating to wood drying process. The thermal efficiency and energy consumption ratio of the two solar dryers named Oxford and Boral have been evaluated regarding the meteorological and location data of Brisbane, in Australia [34,35]. The Oxford kiln is likely to reduce drying time and enable to receive a great quantity of solar energy compared to the Boral kiln. The Oxford design has a drying efficiency of 55% and 40% for the Boral design. The energy consumption for reducing moisture content from 0.53 to 0.15 kg water/dry matter of 10 m^3 wood stack was 182 kWh for the Oxford kiln and 113 kWh for the Boral kiln. Luna et al., [36] carried out a theoretical study to assess the efficiency of solar timber kilns to reduce drying time with and without air renewal. Results found that the judicious use of thermal storage and ventilation seemed to be an efficient way for reducing drying time and allowing good quality of dried wood. Khouya [37] found that the drying time required for a 25 mm thick hardwood board in a solar kiln was 96 h versus 20 h using a conventional vacuum drier and superheated steam [38]. Nevertheless, the disadvantage of solar drying is that the solar irradiation varies according to the months and the days. Solar drying is usually done during the summer period, as it is the season when solar radiation is most important. Thus solar drying would be exploitable and very interesting if it is integrated with a backup system that makes drying continuous and remedy the deficiencies of the sun especially in the evening and rainy days and a solar-assisted heat-pump system that save energy. In present work, a hybrid CPV/T system will be integrated in solar kiln in order to supply the HP and fans with electricity needed. Thermodynamic parameters and thermal performance of a hybrid solar dryer will be analyzed for different operations conditions during the softwood drying process. This proposed drying method will have a positive effect on reducing drying time and increasing the production capacity of the hybrid dryer studied.

For any drying model, the sorption isotherms and the heat and mass transfer coefficients are necessary to establish the numerical simulations and to evaluate the specific moisture extraction rate (SMER) in the material. SMER is a key indicator that measures the ratio of the amount of water evaporated by a hygroscopic solid to the energy consumed during the drying process. Khouya and Draoui [39] evaluated the mass transfer coefficients and sorption isotherms for softwood and hardwood species under different operating conditions using a drying chamber controlled in temperature and relative humidity. Experimental results have shown that the evaporative capacity is fast for Softwood than Hardwood. Food SMER has been shown to be slightly affected by outside temperature and relative humidity in an air/air heat pump dryer operating at a fixed set-point [40]. There is a shortage of scientific studies relating to the SMER of an air/air heat pump during a wood drying process. In addition, the SMER relating to a water/air heat pump integrated in a hybrid solar dryer deserves to be investigated. In this investigation, the SMER of a water/air heat pump will be evaluated for different set-points and outside temperatures. Various existing investigations also evaluate the drying costs using different types of conventional dryers [41,42]. Quesada-Pineda [43] conducted a study at Virginia polytechnic institute and State University to evaluate the electricity costs of wood product manufactories. The results found that the amount of electrical energy consumption to produce Hardwood products ranged from 84 to 111 kWh/MBF (1 MBF of lumber = thousand board feet). The energy consumption ratio related to dry 2.8 m^3 of spruce from initial moisture content of 0.6 to 0.15 kg water/kg dry matter at drying air temperatures ranging from 50 to 80 °C was 3894 MJ (1082 kWh) [41]. Few studies have discussed the impact of thermal regeneration and a humidification process on energy consumption and costs related to the wood drying process [44,45]. In present work, a humidification process will be used for energy saving purpose. It improves the thermal performance of the HP in particular and of the drying system in general.

In the literature survey, it is brought to the attention of the author

that there is a lack in the use of hybrid renewable energy systems during the wood drying process. The present work will propose a CPV/T system as a new hybrid solution for carrying out the drying process of softwood. This work aims to investigate the combined effect of heat pump and concentrated photovoltaic thermal on drying performance of a softwood solar kiln. It will make a technical contribution to industrial dryers that use heat pumps as the main source of energy. In fact, thanks to the integration of a CPV/T system in these dryers, the electrical energy consumption of the water/air HP will be considerably reduced, which will improve the system performance and its added value. This work is constructed as follows: firstly, a report of the methods and materials used to carry out this investigation will be presented. Then, mathematical models to predict the behavior of different units of the combined system will be presented. The drying model equations will be solved using the finite difference method by mean of a subprogram. The numerical simulations will be carried out under Tangier climate, in Morocco. The results of the studied model will make it possible to predict the evolution of heat and mass transfer during the wood drying process using a heat pump and a CPV/T system. Drying parameters such as drying capacity and electrical energy consumption ratio will be evaluated in various drying operations. The effect of certain parameters such as the set-point, concentration ratio, outdoor air temperature, aperture area and the air mass flow rate on the thermal performance of the drying system will be analyzed. This work will conclude with a general conclusion and promising perspectives.

2. Material and method

The thermal performance of a combined drying system is investigated under temperate climate of Tangier city (latitude 35°46′02″ North, longitude: 5°47′59″ West), in Morocco. The synoptic diagram of the drying system is shown in Fig. 1. This system consists of a drying chamber, a water/air heat pump, electrical and hydraulic accessories, a CPV/T system and heat exchangers. The floor, roof and walls of the drying chamber are constructed using a 0.03 m thick wooden frame, in series with 0.02 m thick polyurethane foam. The dryer has a volume of 80 m^3 with a vacuum rate of 0.5. The water/air HP proposed is specially designed for heating hot water of industrial applications. This HP is powered by the CPV/T system and the grid. A regulation system is set up to stop the pump running when its setpoint temperature is lower than that of the outlet air at the CPV/T loop. The concentrated photovoltaic thermal system (CPV/T) is introduced in this investigation in order to satisfy the electrical and thermal need of the drying system. The CPV/T system used has a mirror area of 100 m^2 and a concentration factor of 100. The receiver is equipped with the PV cells (InGaP/GaAs/Ge) and exposed to the solar flux reflected from the mirror. The electrical and thermal energy production remains dependent on the climatic condition in which the CPV/T system is installed. The air coming out of the dryer is wet and hot, which is why a heat recovery system was used to recover some of energy released into the atmosphere. The outdoor air could be preheated first in the Closed Feed Air Heater (CFAH) before being routed to the heat exchangers installed into the drying duct. The air leaving the CFAH is directed to the HP evaporator to transmit heat to the refrigerant flowing through it. The drying system operates in forced convection and defined according to the dimensions of wood stack. The wood specie selected for this study is Spruce (Softwood). It is commonly used in building construction, furnishing and heating systems [46].

3. Mathematical modelling

3.1. Mathematical modelling of the CPV/T system

Numerous studies have been carried out the different applications of the CPV/T system [29,47–49]. Investigations have been proposed a CPV/T to satisfy the need of electricity and heat of an industrial process [29,47]. It was found that high concentration photovoltaic systems could be an important way to massively produce renewable electricity at lower costs [48]. In recent investigation, waste heat recovery from a CPV/T system was used to power an Organic Rankine cycle for residential applications [49]. There is a shortage in the use of CPV/T systems for drying application purposes. In this work, a CPV/T system is proposed to supply the wood dryer with electricity and heat necessary for the proper functioning of its components. Fig. 2 illustrates the schematic diagram of the CPV/T system studied. This system is composed of a parabolic mirror, a receiver equipped with the PV cells, a selective layer, an insulating structure and a pipe in which the coolant circulates. The establishment of the equations governing the heat transfer in different components of the CPV/T system is based on the following assumptions:

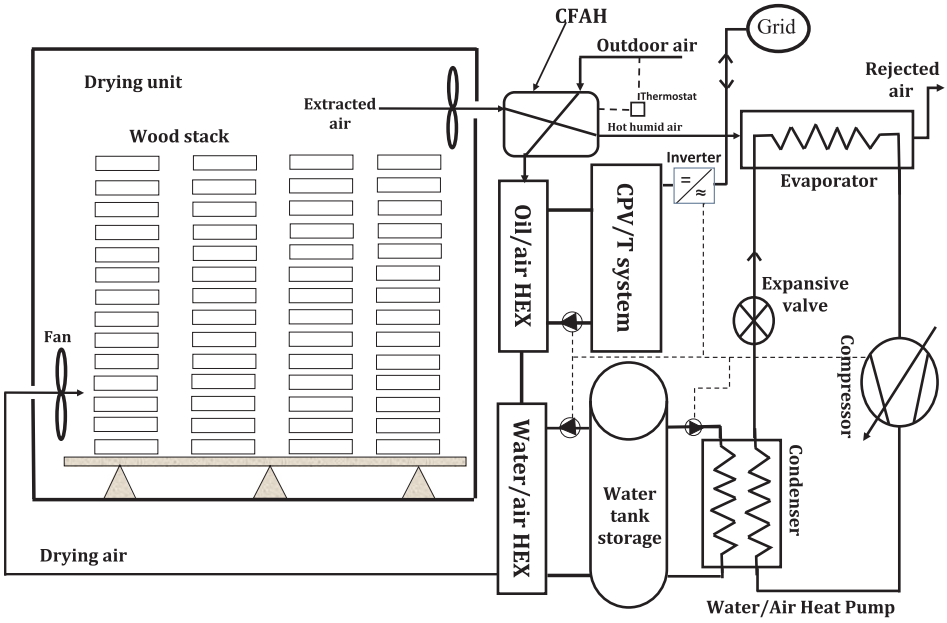

Fig. 1. Schematic diagram of the solar kiln.

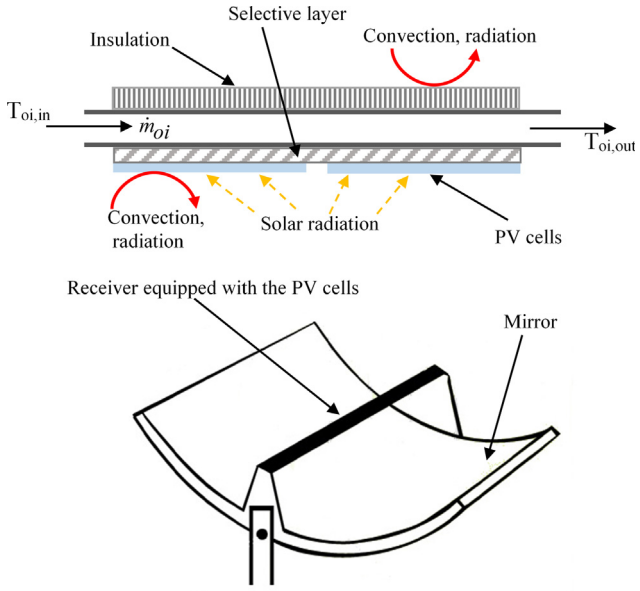

Fig. 2. Schematic diagram of the CPV/T system.

- The thermophysical properties of the CPV/T system are constant;
- The ambient temperature around the receiver is uniform;
- The solar flux at the receiver is uniformly distributed
- The heat transfer is unidirectional;
- The HFT (oil) is incompressible;
- The thermal gradient within the solid is negligible;
- The sun tracking system is perfect.

Given these assumptions, the equations governing the heat transfer in the components of the CPV/T system are described in the following sections.

3.1.1. Thermal balance of the PV cells

The solar energy received by the CPV/T system is converted into electricity and heat. Part of the heat is transferred by conduction to the selective layer and the other part is lost by radiation and convection for the environment benefit. The energy balance for the PV cells is established as [37]:

$$C_r A_{rec} I \eta_{op} \eta_{re} \alpha_{pv} + A_{rec} K_{pv,l}(T_l - T_{pv}) - h_{r,pv,sky} A_{rec}(T_{pv} - T_{sky}) - h_{c,pv,a} A_{rec}(T_{pv} - T_{ae}) - \dot{P}_{el,pv} \approx 0 \quad (1)$$

where $\dot{P}_{el,pv}$ is the electrical power generated by the CPV/T evaluated as [29]:

$$\dot{P}_{el,pv} = A_{pv}.\ I.\ \eta_{op}.\ \eta_{re}.\ \eta_{pv}.\ \eta_{inv}.\ \eta_{\text{mod}} \quad (2)$$

η_{pv} is the PV cell electrical efficiency expressed by Eq. (3) as a function of the concentration factor Cr and the module temperature T_{pv} as [47]:

$$\eta_{pv} = 0.298 + 0.0142 \ln(Cr) + (0.000069 \ln(Cr) - 0.00075)(T_{pv} - 298) \text{ for Cr } < 200 \quad (3)$$

The net electricity production by the CPV/T can be computed using Eq. (4) as [50]:

$$\dot{P}_{el,pv,net} = Cr.\ I.\ A_{pv} \eta_{op} \cdot \eta_{re} \cdot \eta_{pv} \cdot \eta_{inv} \cdot \eta_{\text{mod}} - \eta_{inv} \times \dot{Q}_{par} \quad (4)$$

where $\dot{Q}_{par}$ is the parasitic power consumption for the tracking motors and coolant pump, it is assumed to be 2.3% of the intercepted radiation power.

3.1.2. Thermal balance of the selective layer

In the selective layer, heat transfer takes place only by conduction from the PV cell to this layer itself and then to the pipe. Therefore, the thermal balance can be written simply as [47]:

$$A_{ib} K_{pi,l}(T_{pi} - T_l) + A_{pv} K_{pv,l}(T_{pv} - T_l) = 0 \quad (5)$$

3.1.3. Thermal balance of the pipe

The pipe is heated by conduction through the selective layer then exchanges heat by convection with the cooling fluid then transmits a part of heat by conduction towards the receiver insulating structure. The thermal balance of the pipe is written [37]:

$$h_{c,pi,oi} A_{pi}(T_{oi} - T_{pi}) - A_{pv} K_{pv,pi}(T_{pi} - T_l) - A_{ib} K_{pi,ib}(T_{pi} - T_{ib}) \approx 0 \quad (6)$$

3.1.4. In the pipe heat transfer fluid(oil)

The working fluid circulating in the absorber tube only heats by convection. By adopting the hypothesis of unidirectional heat transfers through the system, the thermal balance for the coolant can be written as [51]:

$$\dot{m}_{oi}.\ C_{p,oi}.\ \frac{dT_{oi}}{dx} = a.\ h_{c,pi,oi}.\ (T_{pi} - T_{oi}) \quad (7)$$

3.1.5. In the insulating structure

In the insulating structure, heat transfer takes place by conduction of the absorbent tube towards this layer itself then to the ambient air. It also exchanges heat by convection and by radiation with the environment. Therefore, the heat balance can be written simply as [37,47]:

$$A_{ib} K_{pi,ib}(T_{pi} - T_{ib}) - h_{r,ib,ae} A_{ib}(T_{ib} - T_{sky}) - h_{c,ib,ae} A_{ib}(T_{ib} - T_{ae}) = 0 \quad (8)$$

In Eqs. (1), (5), (6) and (8), conduction heat transfer coefficient K_{ij} between two adjacent layers i and j can be estimated as [47]:

$$K_{ij} = \frac{1}{\frac{\delta_i}{K_i} + \frac{\delta_j}{K_j}} \quad (9)$$

In Eq. (7), convective heat transfer coefficient between tube and HTF can be evaluated by Eq. (10) as a function the Nusselt number Nu, the air thermal conductivity λ and the pipe hydraulic diameter d as [52]:

$$h = \begin{cases} \frac{\lambda}{d} 4.\ 36 \text{ for laminar flow (Re } < 2300) \\ \frac{\lambda}{d} Nu \text{ for turbulent flow (Re } > 2300) \end{cases} \quad (10)$$

where

$$Nu = \frac{\left(\frac{\chi}{8}\right)(\text{Re} - 1000)\,\text{Pr}}{1 + 12.7\left(\frac{\chi}{8}\right)^{0.5}((\text{Pr})^{2/3} - 1)} \quad (11)$$

χ is the friction factor expressed as:

$$\chi = (1.82 \log_{10}(\text{Re}) - 1.64)^{-2} \quad (12)$$

Re is the Reynolds number calculated as [37]:

$$\text{Re} = \frac{\upsilon V}{D} \quad (13)$$

where ν is the viscosity of the HTF flowing at speed V and D the hydraulic diameter of the pipe.

In Eqs. (1) and (8), convective heat transfer coefficient h_c outside the receiver due to wind speed u can be computed using Eq. (14) as [37]:

$$h_{c,pv,ae} = h_{c,ib,ae} = 2.8 + 3u_{ae} \text{ for } (0 \leqslant u_{ae} \leqslant 7 \text{ m. s}^{-1}) \quad (14)$$

Finally, the radiative heat transfer coefficient between the body i

and the body j of the CPV/T system can be determined as [47,53]:

$$h_{r,i,j} = \frac{\sigma(T_j^2 + T_i^2)(T_j + T_i)}{\frac{1}{\varepsilon_i} + \frac{1}{\varepsilon_j} - 1} \text{(i, j= pv (PV cell), sky or ib (insulation))} \quad (15)$$

The associated initial and boundary conditions are:

$$\text{At\;t} = 0\text{\;:}\; T_{oi} = T_{ae} \quad (16)$$

$$\text{At\;x} = 0\text{:}\; T_{oi} = T_{ae}$$

The equations governing heat transfer in the CPV/T system (Eqs. (1), (5), (6), (7) and (8)) are assembled and solved using the Runge Kutta 4th order method [45]. The program for calculating the CPV/T dynamic parameters was written in C ++ language. At each time iteration, the calculation code makes it possible to determine the temperatures of various components of the system as well as that of the coolant. In this work, synthetic oil was used as the HTF of the system and its outlet temperature remains dependent on several parameters such as its mass flow rate, the concentration factor and the climatic conditions of the solar installation place. This HTF (coolant) which is heated by the CPV/T system will then be led to a heat exchanger in order to transfer the heat to the air used to carry out the wood drying operations. In this work, all calculations relating to heat exchange are performed using the NTU method as described in a previous work [51].

3.2. Water/air heat pump model

In this work, a water/air heat pump was proposed to conduct the softwood drying operations. The heat pump is characterized by an electric power ($\dot{W}_{comp}$) consumed by the compressor to produce the necessary heat ($\dot{Q}_{th}$) from the condenser and raise the water temperature to the set-point required for drying (T_{set}). For a water–air HP, condensation occur indirectly via a closed circuit connecting the machine to the hot water tank (Fig. 1). The hot water produced in the condenser circuit and accumulated in a storage tank is directed to a heat exchanger arranged in the areraulic duct in order to transmit the heat to the drying air. The amount of heat exchanged between air and water depends on their inlet and outlet temperatures, their mass flow rates and the effectiveness of the exchanger used. The heat pump calculation parameters are based on the following assumptions:

1. The HP is suitable for lower outdoor temperatures and can supply hot water at 90 °C. The underlying technology is a Flash injection circuit which, via an Inverter Scroll compressor and a specially designed injection opening, provides the system with the optimum amount of refrigerant needed to set a given set-temperature in the hot water tank based on drying requirements. The nominal operating characteristics of the studied HP are described in Table 1.
2. The temperature of the hot water tank remains constant and can be adaptable according to the drying needs;
3. The thermal losses from the HP circuit to the outside environment are negligible;
4. There is no thermal stratification in the storage tank.

In this work, the multiple linear regression model was used to predict the power consumption of the compressor and the heat added to the condenser. This model is made up of empirical equations correlating the power to the operating parameters such as, rated power, rated and non-nominal outdoor temperature, water temperature in the storage tank. The model introduces the scaling constants for the input parameters. These power variables are determined using the least squares method by exploiting a set of experimental measurements obtained during the water heating using a heat pump. The regression model of compressor and condenser powers for a water/air heat pump is given by Eqs. (17) and (18), respectively, as [23,54]:

$$\dot{W}_{comp,AC} = \dot{W}_{comp,nom}\cdot(\omega_1 + \omega_2(T_{ev,a,in} - T_{ev,a,nom}) + \omega_3(T_{set,w,AC} - T_{set,w,nom}) + \omega_4(T_{ev,a,AC} - T_{ev,a,nom})(T_{set,w,AC} - T_{set,w,nom})) \quad (17)$$

$$\dot{Q}_{th,AC} = \dot{Q}_{th,nom}\cdot(\omega_1 + \omega_2(T_{ev,a,in} - T_{ev,a,nom}) + \omega_3(T_{set,w,AC} - T_{set,w,nom}) + \omega_4(T_{ev,a,AC} - T_{ev,a,nom})(T_{set,w,AC} - T_{set,w,nom})) \quad (18)$$

ω_1, ω_2, ω_3 and ω_4 are scaling constants determined by test in previous work [23,54]. The scaling constant values are given in Table 2. $\dot{W}_{comp,nom}$, $\dot{Q}_{th,nom}$, $T_{ev,a,nom}$ and $T_{set,w,nom}$, are input parameters to the system.

The thermal energy that the heat pump must transfer to the drying system strongly depends on the tank temperature (here, air leaving the regenerator of the hybrid solar dryer) in which the evaporator extracts the heat. Experiments have shown that the heat pump consumes less electrical energy when the temperature difference between the hot and cold sources is not large [54]. For this reason, geothermal heat pumps (ground source HPs) have better performance than their counterparts relying on outside air to transfer heat to the evaporator [55]. The HP coefficient of performance which expresses the ratio between the actual heat power added to the condenser and that consumed by the compressor is given by Eq. (19) as [16]:

$$COP = \frac{\dot{Q}_{th,AC}}{\dot{W}_{comp,AC}} \quad (19)$$

As mentioned in previous section, the HP evaporator exchanges heat with the hot humid air leaving the dryer, thus the electrical consumption will be reduced and the COP will be considerably improved. In this sense, it should be noted that the temperature evolution of air in the regenerator and evaporator units is evaluated using the energy balance on the Closed feed air Heater as described in previous work [37,45].

In this work, an approach for reducing the heat pump energy consumption was considered. The compressor will be switched off when the air temperature at the outlet of the exchanger supplied by the CPV/T system is higher than that of the set-point T_{set}. In practice, it is a smart meter which records the electrical energy consumption of the compressor of the heat pump accessories (thermostat, pump, fans, …). As the temperature of air leaving the HEX reaches T_{set}, the hydraulic pump must automatically stop the circulation of hot water. In the event that no thermal loss occurs in the HP circuit, the heat released at the hot water tank can be considered proportional to that trapped by air in drying duct and the electrical energy consumption of the compressor can be estimated based on the following approach:

$$E_{comp} = \int_0^t \frac{\dot{Q}_{ex}}{COP} dt \quad (20)$$

where:

$$\dot{Q}_{ex} = \begin{cases} \varepsilon.\, Q_{max} \text{ if } T_a \leqslant T_{set} \\ 0 \text{ if } T_a \geqslant T_{set} \end{cases} \quad (21)$$

Table 1
Heat pump characteristics.

Nominal settings	Values
Outdoor temperature (K)	280
Return temperature (K)	338
Starting temperature (K)	288
Water mass flow rate (L.min^{-1})	11.2
Condenser power (kW)	40
Compressor (Hermetic Scroll) (kW)	11.5
Fans (kW)	0.92
COP	3.44
Refrigerant fluid type	CO_2 (R744) 6.5 kg
Heat exchanger	Serpentine (copper)
Pump (kW)	0.1

Table 2
Scaling constant values of HP model.

Scaling constants	ω_1	ω_2	ω_3	ω_4
Electrical power	1	0.024	−0.003	−0.0005
Thermal power	1	0.005	0.017	0.00011

This regulatory approach means that for $T_a \geq T_{set}$, the drying is carried out only by the hot air produced using the CPV/T system. The total electrical energy consumption of the heat pump must integrate throughout the drying period, the powers absorbed at each operating speed of all the elements consuming energy such as fans, pumps and other auxiliaries. The overall electrical consumption of the HP during a drying period is:

$$E_{el,HP} = E_{comp} + E_p + E_{np} + E_d (kWh) \quad (22)$$

In Eq. (22), E_p is the energy consumption of the permanent auxiliaries (fans, pumps, etc.) and non-permanent auxiliaries E_{np} (crankcase resistors, etc.), respectively. E_d is the consumption linked to the possible defrost, it also increases the heat requirements which will have to be compensated by an additional operation of the compressor.

3.3. Mathematical modelling of the drying unit

3.3.1. Assumptions

The physical drying model typically includes several partial differential equations such as the mass balance equation, the heat balance equation, the heat transfers and the drying rate equations. All these equations are developed to describe the heat and mass transfer between drying air and wood, as well as in a single slice of the product during a time step Δt. The governing heat and mass transfer equations are based on the following assumptions [23,37,51,36,56]:

- The wood stack consists of a number of boards arranged horizontally in the longitudinal direction;
- Each board is divided into N slices numbered from 0 to N-1 according to the thickness and in the direction of the mass air flow;
- Heat and mass transfers are unidirectional;
- The air velocity is uniform along the boards;
- The mass flow rate of hot air is diffused equitably at the entrance area of the wood stack;
- The characteristics of the air at the exit of a wood board are considered as conditions of entry into the next board;
- The heat losses of the drying chamber to the environment are negligible;
- The conditions of the air leaving the dryer are the same as those at the entrance of the CFAH;
- The equilibrium water content between wood and the environment exists and depends on the relative humidity and the air temperature.

By adopting all the above assumptions, the drying model equations are expressed below.

3.3.2. Drying model

The drying air with a mass m_a leaves the water–air heat exchanger at temperature T_a and a water content W_a. It transmitted heat by convection to the segment of wood arranged in the column. On the other hand, drying air sees its absolute humidity increases due to the evaporation which manifests itself in the product. This drying air flows crosses the wood segment section at the velocity u_a. The heat and mass transfers of drying air in contact with a first wood slice (segment 0) can be expressed using Eqs. (23) and (24), respectively, as described in previous work as [56]:

$$\frac{1}{2} m_a \, C_{p,a} \frac{dT_a}{dt} = \frac{1}{2} u_a A_s \rho_a C_{p,a} (T_{a,in} - T_{a,out}) - h_{th} A_s (T_a - T_{A0}) + \Delta H A_s K_g (X_{sat} - X_{eq}) \quad (23)$$

$$\frac{1}{2} m_a \frac{dW_a}{dt} = \frac{1}{2} u_a A \rho_a (W_{a,in} - W_{a,out}) + \Delta H A K_g (X_{sat} - X_{eq}) \quad (24)$$

K_g is the overall mass transfer coefficient ($kg.m^{-2}.s^{-1}$) given by the expression [51]:

$$\frac{1}{K_g} = 0.2265 \exp\left(\frac{2543.6}{T_a}\right) e + 268.9 \exp\left(\frac{2543.6}{T_a}\right) u_a^{-2.72} . \exp\left(-\frac{1 - RH}{X_{psf} - X_{eq}}\right) \quad (25)$$

X_{eq} is the equilibrium moisture content computed as [37]:

$$X_{eq} = (b_1 X_m RH)/(1 - b_2 RH)(1 - b_2 RH + b_1 RH)) \quad (26)$$

where:

$$RH = \frac{W_a P_{atm}}{(W_a + 0.622) P_{vs}(T_a)} \quad (27)$$

$$b_1 = 27.73 \exp(-2135.87/(RT)) \quad (28)$$

$$b_2 = 1.93 \exp(-2308.79/(RT)) \quad (29)$$

$$X_m = -7.\ 3310^{-4} T + 0.286 \quad (30)$$

X_{psf} is the fiber saturation point expressed as:

$$X_{psf} = (b_1 X_m)/((1 - b_2)(1 - b_2 + b_1)) \quad (31)$$

It should be noted that the boards consist of anhydrous wood (mass M_0) and water in the liquid or adsorbed state (mass $X.M_0$). The thermal capacity of a wood board is equal to the sum of the thermal capacities of anhydrous wood ($M_0 C_{p,0}$) and water ($X\ M_0 C_{p,w}$). During drying, the moisture content X varies due to the evaporation that occurs in the product. On the other hand, the anhydrous mass of the product M_0 remains constant and the rate of heat transfer associated with the evaporation of water in the wood segment is equal to $\Delta H A_b K_g (X_{sat} - X_{eq})$. The heat transfer rate equation on the wood segment 0 can be written as [56]:

$$\rho_b V_{A0} \, (M_0 C_{p,0} + X M_0 C_{p,w}) \frac{dT_{A0}}{dt} = \dot{m}_w |_{A1}^{A0} A_b C_{p,w} (T_{A1} - T_{A0}) - \dot{Q}_K |_{A0}^{A1} + h_{th}.\ A_c (T_a - T_{A0}) - \Delta H.\ A_b.\ K_g. (X_{sat} - X_{eq}) \quad (32)$$

In Eq. (3), $\dot{m}_w$ is the specific mass flow of water computed using Eq. (41) as [52]:

$$\dot{m}_w = \rho_w D_w \ |\nabla X| \quad (33)$$

In Eq. (33), the water diffusion coefficient D_w is computed using Eq. (34) as:

$$D_w = \mu D_a \quad (34)$$

D_a and μ are respectively the vapour diffusion coefficient and the relative liquid permeability expressed as:

$$D_a = 2.226.\ 10^{-5} \frac{1}{P} \left(\frac{T + 273}{273}\right)^{1.81} \text{ where p is the pressure} \quad (35)$$

$$\mu = 2 + \left(\frac{X}{X_{sat}}\right)^2 \left(-3 + 2\left(\frac{X}{X_{sat}}\right)\right) \quad (36)$$

The second term of the right member in Eq. (32) represents the conduction heat within the board expressed as:

$$\dot{Q}_K = K_b A_s \ |\nabla T| \quad (37)$$

In the same way, the mass balance equation on the wood segment 0

is written as [37,51,56]:

$$\rho_b V_{A0} \frac{dX_{A0}}{dt} = \dot{m}_w|_{A1}^{A0} A_b - \Delta H A_b K_g (X_{sat} - X_{eq}) \quad (38)$$

For all segments of wood numbered from 1 to N-2, the heat and mass transfer can be expressed by Eqs. (39) and (40), respectively, as:

$$\rho_b V_{Ai} (M_0 C_{p,0} + X M_0 C_{p,w}) \frac{dT_{Ai}}{dt} = \dot{m}_w|_{Ai+1}^{Ai} A_b C_{p,w} (T_{Ai+1} - T_{Ai}) - \dot{m}_w|_{Ai}^{Ai-1} A_b C_{p,w} (T_{Ai+1} - T_{Ai}) + \dot{Q}_K|_{Ai-1}^{Ai} - \dot{Q}_K|_{Ai}^{A1+1} \quad (39)$$

$$\rho_b V_{Ai} \frac{dX_{Ai}}{dt} = \dot{m}_w|_{Ai+1}^{Ai} A_b - \dot{m}_w|_{Ai}^{Ai-1} A_b \quad (40)$$

The conservation equation of heat and mass for the last wood segment can be determined by Eqs. (41) and (42) as:

$$\rho_b V_{AN-1} (M_0 C_{p,0} + X M_0 C_{p,w}) \frac{dT_{AN-1}}{dt} = -\dot{m}_w|_{AN-1}^{AN-2} A_b C_{p,w} (T_{AN-1} - T_{AN-2}) + \dot{Q}_K|_{AN-2}^{AN-1} \quad (41)$$

$$\rho_b V_{AN-1} \frac{dX_{AN-1}}{dt} = -\dot{m}_w|_{AN-1}^{AN-2} A_b \quad (42)$$

The drying model equations are solved using the implicit finite difference scheme and Thomas Algorithm with a convergence criterion of 10^{-6} [37,51,57]. The time and space step are equal to 100 s and 0.00125 m, respectively. A C++ code language has been used in order to find the evolution of moisture content and temperature in wood stack, inside and outside drying air temperature, absolute and relative humidity of air. The drying model also makes it possible to estimate after each iteration the drying parameters such as the energy consumption ratio and the drying efficiency of the system.

3.4. Performance model

The performance of the drying system is evaluated in terms of parameters such as the drying efficiency η and the specific moisture extraction rate (SMER). Drying efficiency is defined as the rate of heat energy required to evaporate water from the initial moisture content until the boards reach equilibrium moisture content by the thermal energy supplied to the dryer [45]:

$$\eta = \frac{m_w.\ \Delta H + m_w.\ C_{p,w}(T_{w,fi} - T_{w,i})}{Q_u + P_{fans}} \quad (43)$$

where Q_u is the useful energy transferred to the drying chamber computed using Eq. (44) as a function of the air mass flow rate m_a, the air heat capacity $C_{p,a}$ and air inlet and outlet temperature at the water/air heat exchanger as [37]:

$$Q_u = \int_0^{t_{dr}} \dot{m}_a.\ C_{p,a}.\ (T_{HEX,a,out} - T_{HEX,a,in}) dt \quad (44)$$

P_{fans} is the fans electrical energy consumption (kWh).

The specific moisture extraction rate ($kg.kWh^{-1}$) related to the use of the heat pump is computed using Eq. (45) as the ratio between the mass of removed water m_w and the electrical energy consumed during the drying process [58]:

$$SMER = \frac{m_w}{E_{el,HP}} \quad (45)$$

The moisture extraction rate ($kg.h^{-1}$) is evaluated using Eq. (46) as the ratio between the removed water m_w and the drying time required for the process [58]:

$$MER = \frac{m_w}{t_{dr}} \quad (46)$$

Table 3
Parameters of the CPV/T.

Parameter	Value
Design parabolic trough:	
Aperture area (m^2)	100
PV Cell (InGaP/GaAs/Ge):	
Thermal conductivity ($W.m^{-1}.K^{-1}$)	50
Module efficiency (-)	0.9
Optical efficiency	0.9
Reflector and inverter efficiency	0.9
Concentration ratio	100
Heat transfer fluid:	
Density ($kg.m^{-3}$)	875
Flow rate ($kg.s^{-1}$)	0.5

3.5. Calculation methodology

In this work, a stack of Spruce with an initial moisture content of 0.8 kg water/kg dry matter is considered. Each board has a dimensions of 2 m × 0.2 m × 0.025 m. The dryer has a volume of 80 m^3 with a vacuum rate of 0.5, thus, the volume of wet wood is 80 × 0.5 = 40 m^3 and its initial mass M_i = 450 kg/m^3 × 40 m^3 = 18000 kg. The distance between two adjacent layers is taken equal to 0.025 m and the total surface area of the boards is S_b = 3640 m^2. The drying is achieved when the moisture content of wood reaches 0.15 kg water/kg dry matter, a final stack weight of M_f = 11500 kg. Therefore, the amount of water that must be released during drying is determined as M_i-M_f = 6500 kg. The mass flow rate and collector area values used in the design of the drying system are 0.6 $kg.s^{-1}$ and 100 m^2 respectively. The receiver equipped with the PV cells has a total area of 1 m^2 which give a concentration factor of 100. Table 3 decline the parameters design of the CPV/T system used to establish the numerical simulations during the wood drying process. The input data requested by the constructed code such as weather conditions and sorption isotherms of wood were brought into play stat variables. The numerical simulations are conducted under Tangier climate, in Morocco. The calculations are made especially by referring to the weather conditions on the 15th day of each month. Table 4 provides some weather conditions for different months. The electrical energy consumption of ventilation (permanent extraction and blowing) can be estimated as follow [59]:

$$E_{fans} = \dot{m}_a \Delta P \frac{t_{dr}}{\eta_{fans}} \quad (47)$$

In this work, two modes according to the drying system functioning are studied:

- Drying method 1: In this mode, the heat pump alone assumes the drying operation during all months. It is powered fully by the electrical grid. The set point in the HP water tank is assumed to be 65 °C. In addition, the CFAH efficiency is assumed to be 0.6. Efficiency equal to 0.6 means that the heat transfer rate achieves 60% of the maximum heat transfer rate, i.e. the amount of heat transferred under the assumption of infinite heat transfer area. The outer shell of CFAH is generally well insulated to avoid any loss of heat in the surrounding environment. Therefore, the thermal energy not transferred by the hot air leaving the dryer to the air coming from outside in the CFAH is used to heat the refrigerant flowing in the evaporator circuit.

- Drying method 2: The strategy of this drying method assumes that the CPV/T assists the HP during the wood drying process, moreover, ε_{reg} = 0.6. In addition, the HP stops working if the outlet air temperature at the collector loop HEX is higher than T_{set}. It should be noted that the electricity produced by the CPV/T system is used to supply the heat pump, its accessories and the fans. This study will also assess the large amounts of electrical energy that the drying system can save when the heat pump and the CPV/T are combined. It should be noted that the electrical energy generated by the CPV/T is directed to an inverter in order to ensure production as needed. Two situations can

Table 4
Weather conditions for different months.

	January	February	March	April	May	June	July	August	September	October	November	December
T_{max} (K)	290	293	295	298	300	306	310	307	300	298	295	292
T_{min} (K)	277	283	288	293	295	296	298	297	291	289	286	280
I_{max} (W.m^{-2})	415	560	620	700	820	1000	1050	1008	890	735	640	500

arise for the inverter operation:

- connect to the network to supplement energy demand when green electricity no longer meets demand;
- to inject the surplus energy into the grid when production exceeds needs. The net invoicing will be settled following the difference between consumption and injection recorded using an electric competitor installed for this purpose.

3.6. Validation of the CPV/T and drying models

Fig. 3 shows the comparison results of the electrical and thermal efficiency of the CPV/T system between the current model and those predicted in previous work [50]. The simulations were established for a concentration ratio of 200 and a solar intensity of 900 W.m^{-2}. The results show that the electrical efficiency of the PV cells decreases as the HTF outlet temperature at the solar collector increases. The thermal efficiency also increases as the HTF temperature increases. The discrepancies between these two models do not exceed 6%. Fig. 4 presents the experimental and numerical evolution in moisture content and drying air temperature during the wood drying process in a conventional kiln. The experiment was carried out in Suifenhe located in a Japanese region with high relative humidity (44°38′N131°17′E) [44]. The tested volume of wood was 50 m^3 with an initial moisture content of 0.4. The air temperature fluctuating between 323 and 329 K. It was found that the lumber reached the equilibrium moisture content of use 120 h after dry. The discrepancy between predicted and measured values does not exceed 4% for both moisture content and temperature. Thus, the perfect agreement indicates that the present drying model is suitable for calculating the drying parameters under different operating conditions.

4. Results and discussion

4.1. Drying softwood with heat pump alone (drying method 1)

The main purpose of a drying operation is to remove the water from the wet product. During the drying operation, there is a double transfer, thermal and mass. The drying air enters the dryer at a very low absolute humidity and leaves it at a higher humidity while its dry temperature decreases. For its part, the water content of the product decreased and its dry temperature increased. The use of heat pumps for drying food has become a common technique in recent years due to the energy required for a drying operation and the increase in energy cost in recent decades [60,61]. Wood as a hygroscopic material is an interesting material for drying with heat pumps [62]. The performance of a heat pump used for drying is measured using two essential indicators which are the energy consumption per kilogram of water released in the product and its energy efficiency which is defined by the ratio useful energy to input energy. The latter is none other than the performance coefficient which depends on several factors such as the temperature of the hot source and the cold source.

In this work, the thermal performance of the drying system using a water/air heat pump as the main heating device is evaluated in term of metric parameters such as the electrical energy consumption ratio (ECR) and the coefficient of performance (COP). Fig. 5 shows the evolution of these parameters during the drying process of softwood using a water/air heat pump as the main heater device. The results show that the ECR reduces by moving from January to July, then increases thereafter. The month of January shows a significant electricity consumption and that of July meanwhile records a low consumption. The ECR fluctuates between 29 and 52 kWh.m^{-3}. It has been found that the ECR (fans + HP) consumed to release 19000 kg of water from a softwood stack of 354 m^3 by using two heat pumps integrated with steam coils was about 23 kWh.m^{-3} [16]. The results demonstrate that the coefficient of performance (COP) increases from January to July, then decreases thereafter. The COP values ranges from 4.97 to 5.6. It has been demonstrated that for a conventional drying process combined with a heat pump, the fans consume about 20 kW and the compressor consumes 84 kW when supplying 446 kW of heat to the drying chamber, therefore, the COP value is 4 [16]. The drying time, MER and SMER for all months considered are indicated in Table 5. The results show that the drying time is shorter in July (hottest month) and longer in January (coldest month). This difference can be explained by the weather conditions which is different from one month to another. The results show that the MER and SMER are increased by going from January to July then decreased thereafter. The maximum values of MER and SMER are 8 kg.h^{-1} and 14.32 kg. kWh^{-1}, respectively. It has been reported that the drying time, MER and SMER for reducing moisture content from 0.45 to 0.05 kg water/dry matter of 1154.4 kg wood stack was 560 h, 0.67 kg.h^{-1} and 0.25 kg.kWh^{-1}, respectively [62].

The effect of outdoor air temperature on SMER and COP during the softwood drying process is also investigated. Figs. 6–8 show the evolution of SMER, COP and T_{ev} according to the outdoor air temperature for different set-points during the softwood drying process. In general, the SMER value increases as the outdoor air temperature and the set-point increase. For an outdoor air temperature of 298 K, the SMER values are 6.16, 6.79 and 7.38 kg.kWh^{-1} for the set-temperatures of 328, 338 and 348 K, respectively. It has been shown that the SMER to release 19000 kg of water by combining HP and the steam boiler was 2.52 kg.kWh^{-1} [16]. The results show that the coefficient of

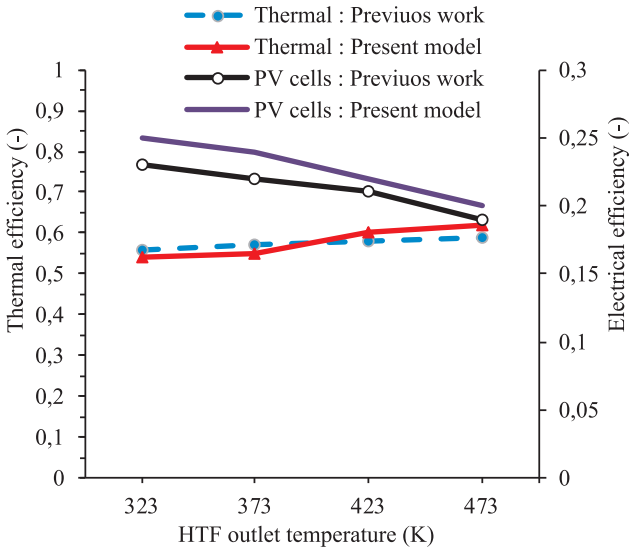

Fig. 3. Variation in electrical and thermal efficiency according to the HFT outlet temperature.

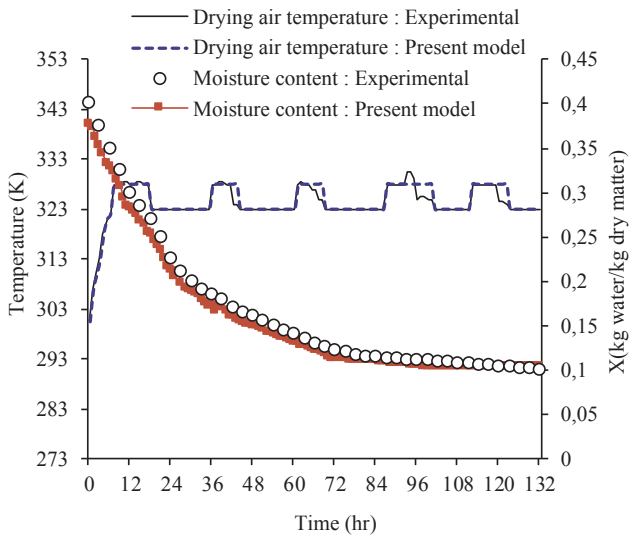

Fig. 4. Variation of moisture content and temperature against time.

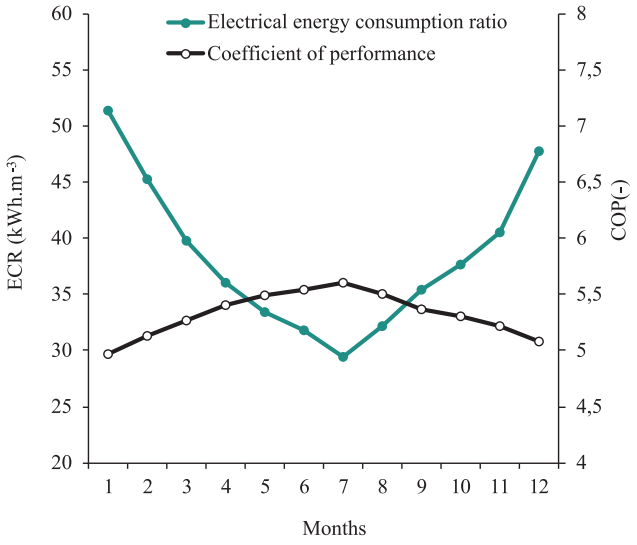

Fig. 5. ECR and COP versus month for Tset = 338 K.

performance increases as the outdoor air temperature increases and the set-temperature decreases. For an outdoor air temperature of 298 K, the COP values are 6.6, 5.45 and 4.6 for the set-temperatures of 328, 338 and 348 K, respectively. These results show that a decrease of the heat pump set temperature from 75 to 65 °C improves the coefficient of performance by at least 17%. In Fig. 8, it is clear that the inlet air temperature in the evaporator increases as the outdoor air and the set-point temperatures increase. For an outdoor air temperature of 298 K, the temperature of air entering the evaporator is 309, 313 and 318 K for the set-temperatures of 328, 338 and 348 K, respectively.

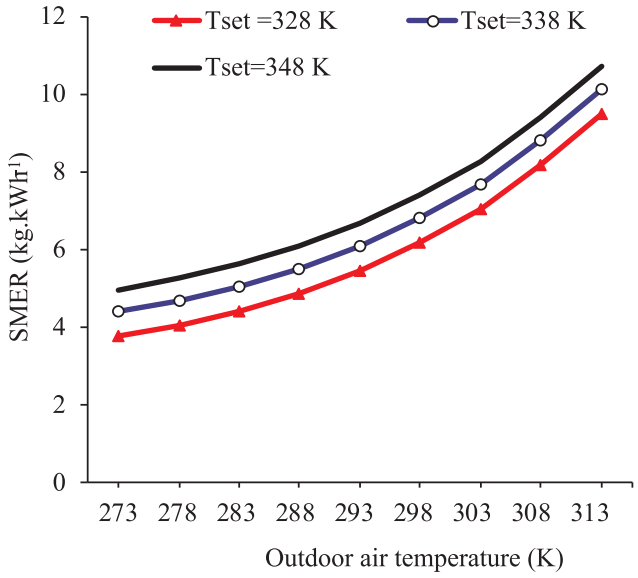

Fig. 6. SMER versus outdoor air temperature for different set-point temperature.

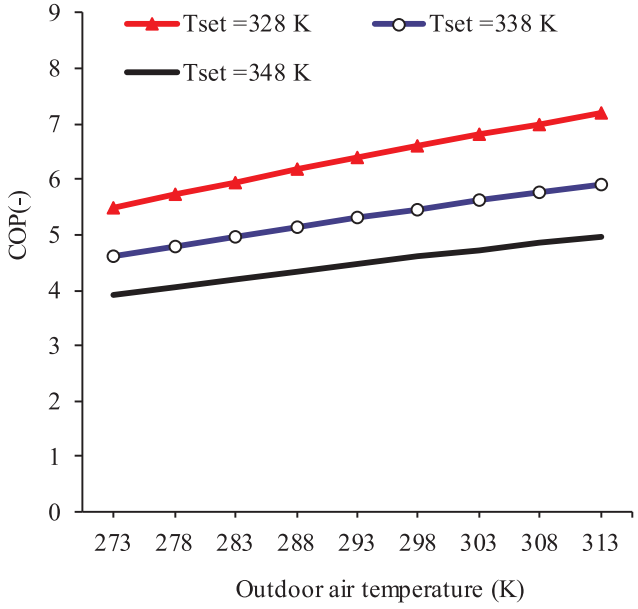

Fig. 7. COP versus outdoor air temperature for different set-point temperature.

4.2. Combined effect of CPV/T and HP on drying performance of a softwood kiln (drying method 2)

In the previous section, the drying performance is evaluated for a dryer operating with a water / air heat pump. In the next section, an innovative solution which consists of integrating a CPV/T system in the kiln to produce the heat and electricity necessary for conducting wood drying operations is proposed. The hybrid dryer studied works thanks to the combination of a CPV/T system and a water/air heat pump. In

Table 5
Parameters evaluated using the heat pump as the main heating device during the Softwood drying process.

	January	February	March	April	May	June	July	August	September	October	November	December
Drying time (h)	578	557	527	523	514	492	453	499	509	512	522	571
MER (kg/h)	11.23	11.66	12.32	12.40	12.6	13.2	14.32	12.9	12.77	12.67	12.44	11.36
SMER (kg/kWh)	4.24	4.59	5.56	6.34	7.03	7.84	8	7.34	6.41	5.94	5.4	4.47

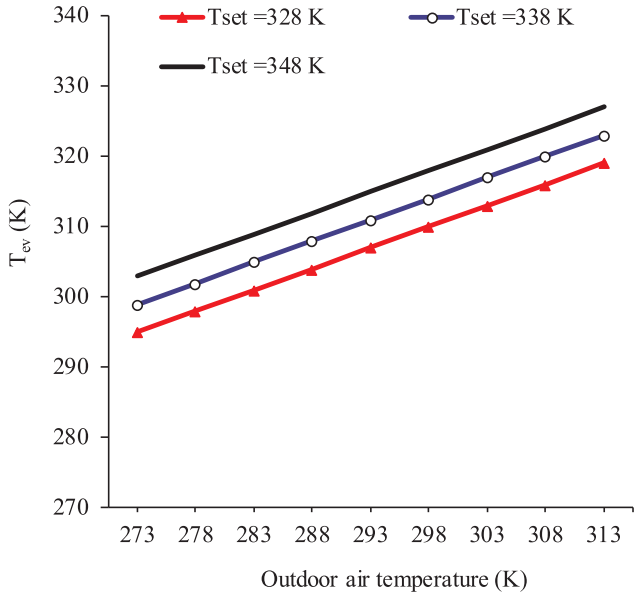

Fig. 8. Effect of the outdoor air temperature on that of the evaporator for different set temperatures.

this investigation, the green electricity generated by the CPV/T is used to power the heat pump, while the thermal energy produced is used to heat the air in an oil/air heat exchanger installed in the drying duct (see Fig. 1). The heated air is then directed to the water/air heat exchanger of the heat pump to undergo the second reheating before being conveyed to the drying chamber.

The thermal performance of the hybrid drying system is evaluated in term of metric parameters such as, the electrical energy produced by the PV cells, the electrical energy consumption by the dryer and that injected into the grid. The evolution of all these mentioned parameters are presented in Fig. 9. The results show that the electrical energy production increases from January to July then decreases thereafter. The monthly electrical energy production fluctuates between 2.08×10^3 and 8.25×10^3 kWh. It was shown that the monthly production of electrical energy by a CPV/T system with a mirror area of 3×40 m^2 was 4.68×10^3 kWh [29]. The results also demonstrated that the electrical energy consumption (fans, pumps…etc.) decreases by going from January to July then increases thereafter. The ECR values vary from 3.96 to 32 kWh.m^{-3}. These results can be explained by the fact that the drying time decreases as the drying air temperature increases [37]. In fact, in July, the CPV/T system receives more sunshine and the temperatures harvested at the oil/air heat exchanger are high enough to carry out the wood drying operations. These higher temperatures have the effect of reducing the drying time and the energy consumption of the water/air heat pump. Conversely, in January, the solar irradiation is weak and the temperatures collected in the CPV/T system are insufficient to carry out the drying. During this period, the thermal energy is mainly produced by the heat pump currently operating at the 65 °C set point. The results show that the drying method 2 allows a reduction of 39 and 86%, in terms of electrical energy consumption comparing to the drying method 1 (HP alone), in January and July, respectively.

The results also show that the electrical energy injected into the grid increases from January to July then decreases thereafter. The energy surplus throughout the year fluctuates between 0.25×10^3 and 7.37×10^3 kWh. It is assumed in section 3.6 that the additional electrical energy to carry out the drying process could be provided by the network, but, these results show that no electrical energy is supplied by the network to complete the drying. Thus, the method proposed for carrying out the wood drying operations seems to be an innovative, efficient, hybrid solution that respects the environment. To check the relevance of the proposed drying method, it is considered useful to compare the current energy consumption ratio with that reported in the literature. Table 6 presents a performance comparison of the proposed solution with that of conventional dryers. It should be noted that the conventional dryers presented for comparison operate using electrical resistors and fans. Although the dryer presented by Ananias et al., [63] operate at higher drying temperatures (358–403 K), it emerged that the ECR of the current model is low compared to this conventional model. In addition, it is interesting to note that the drying temperatures of the present model (328–373 K) greatly exceed that of the conventional model presented by Meng et al., [44]. As described in Fig. 9, with the exception of the months of January and December which have respectively ECRs of 32 and 29 kWh.m^{-3}, drying conducted during the remaining months produces dried wood at an ECR of less than 24.2 kWh.m^{-3}, a value found by Meng et al., [44]. The overall results show that the present model offers better drying performance compared to the conventional dryers presented for comparison.

In Fig. 10, the temperature effect of air leaving the dryer on the humidification and regeneration heat is presented. The results show that the recovered air temperature increases as the temperature of air leaving the dryer increases. For an air temperature leavening the dryer of 360 K, the air inlet temperature in the evaporator is 325 K. This humidification process has probably a significant effect on the HP electrical energy consumption and eventually on the COP. The results also show that the power recovered through the thermal regeneration process increases drastically as the temperature of recycling air increases. In fact, the power recovered increases by 80% when the air temperature leaving the dryer increases from 325 to 365 K. These results are extremely important.

The effect of certain drying parameters on drying capacity and electrical energy consumption ratio during the softwood drying process is also investigated. As a reminder, monthly drying capacity is defined as the total volume of wood that can be dried in a given month. The energy consumption ratio is a key indicator when we want to compare the energy cost price of dried wood with different energy sources used. Therefore, the rationalization of energy consumption consists of contributing to the improvement of this factor and reducing it further, which could open the way to fair competition, especially in the case of a high value-added company operating in the wood drying sector. Fig. 11 shows the evolution in drying capacity and energy consumption ratio (ECR) for different optical efficiency values during the drying process, in December and June. The results show that the ECR increases as the optical efficiency increases. The ECR values are also lower in June than in December. This can be explained by the fact that when the optical efficiency increases, the outlet oil temperature at the CPV/T is

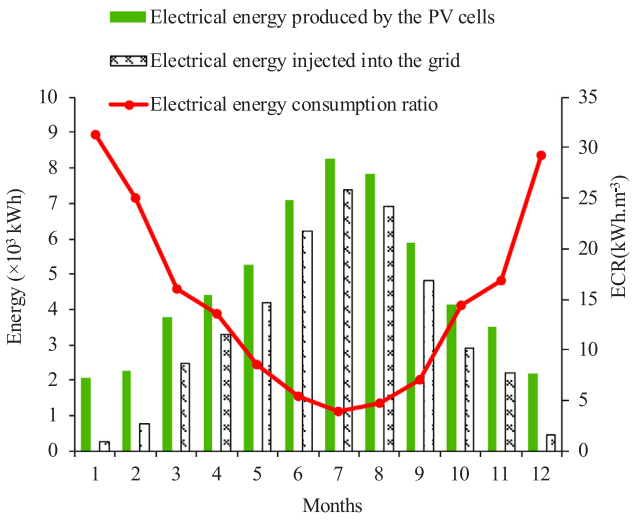

Fig. 9. Variation in energetic parameters depending on the month.

Table 6
Performance comparison of the proposed solution with that of conventional dryers.

	Energy source	X_i (X_f) Kg water/kg dry matter	Drying temperature (K)	Energy consumption ratio (kWh.m^{-3})
Present work	CPV/T + HP water/air	0.8 (0.15)	328–373	4–32
Previous work [63]	Conventional	1.45 (0.1)	358–403	18–120
Previous work [44]	Conventional	0.4(0.10)	318–333	24.2

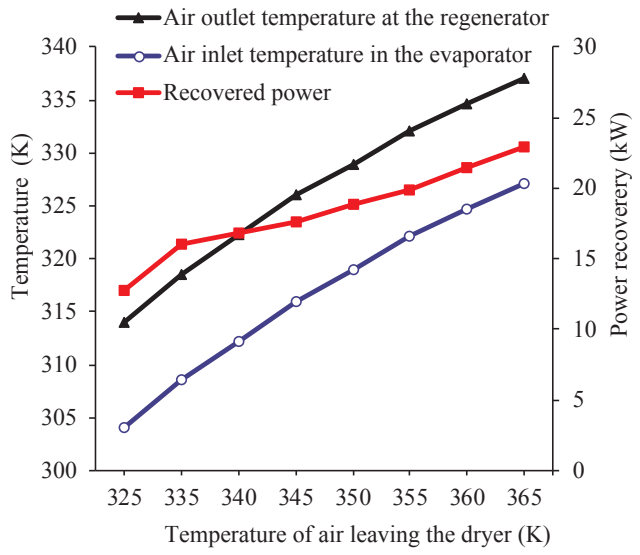

Fig. 10. Effect of return air temperature in the dryer on that of the regenerator and the evaporator.

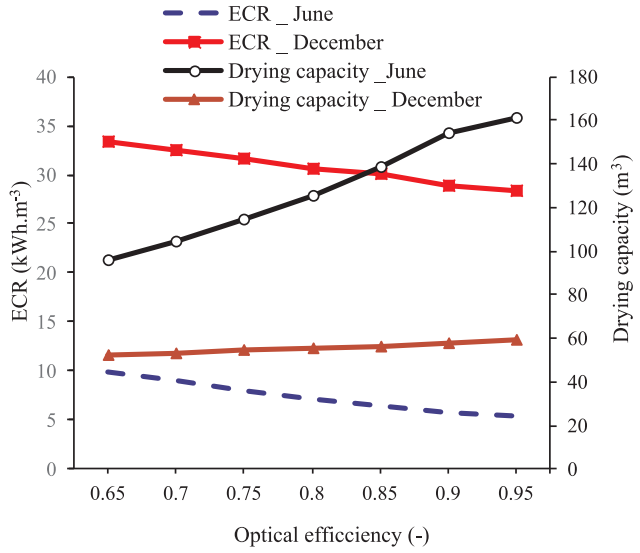

Fig. 11. ECR and drying capacity versus optical efficiency.

important, which reduce the drying time and consequently the ECR. For an optical efficiency of 0.9, the ECR values are 28.8 and 5.74 kWh.m^{-3}, in December and June, respectively. In Fig. 11, it is also demonstrated that the drying capacity increases as the optical efficiency increases. This result is obvious since the thermal energy supplied to the dryer increases as the optical efficiency increases, which reduce consequently the drying time and improve the drying capacity. For an optical efficiency of 0.9, the monthly drying capacity is 58 and 154 m^3, in December and June, respectively. These results indicate that a decrease in optical efficiency from 0.9 to 0.65 increases the electrical energy consumption ratio by 73%, in June.

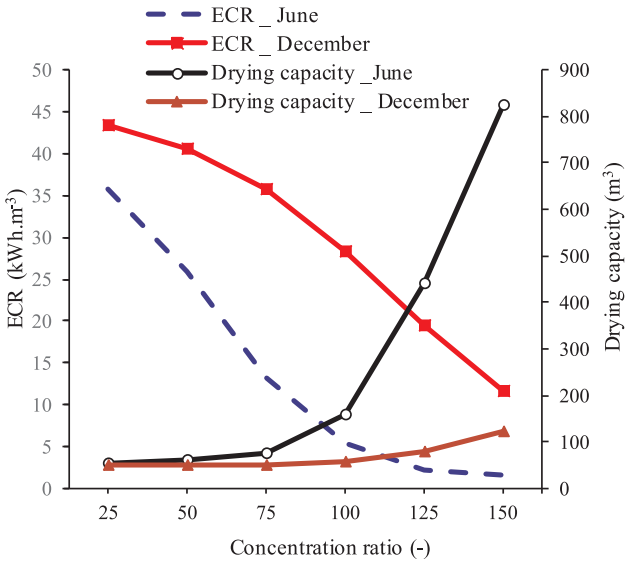

Fig. 12. ECR and drying capacity versus concentration ratio.

The effect of concentration factor on drying parameters is illustrated in Fig. 12. The results show that the ECR decreases as the concentration ratio increases. The results also show that the drying capacity increases as the concentration ratio increases. For a concentration factor of 150, the monthly drying capacity and ECR values are 824 m^3 and 1.55 kWh.m^{-3}, in June, respectively. These results show that the integration of the solar collector with the heat pump is more beneficial in summer than winter because the temperatures harvested at the CPV/T system are insufficient to achieve drying during the coldest months. However, this problem of too long drying time in winter would have been resolved by incorporating a latent storage unit into the drying system as described in a previous work [37].

An important parameter on which the question is decided now is related to the effect of air mass flow rate on drying capacity and ECR. Fig. 13 shows the evolution in drying capacity and ECR for different air mass flow rate values during the softwood drying process. The results show that the drying capacity is higher in June than in December. The results also show that the drying capacity in June increases as the mass air flow increases until reaching a maximum value of 161 m^3 at 0.6 kg.s^{-1} then decreases thereafter. For all the mass air flows considered, the ECR is also low in June than in December. These results are obvious because the climatic conditions of June are generally more favorable for successful drying than those of December [22,45,51]. For an air mass flow rate of 0.6 kg.s^{-1}, the monthly drying capacity and ECR values are 59 m^3 and 29 kWh.m^{-3}, in December, respectively. The results demonstrated that the ECR increases by about 43%, increasing the mass flow rate from 0.6 to 1 kg.s^{-1}, in December. It should be noted that the choice of a mass flow rate conditions the air velocity used to carry out the drying process of wood. As demonstrated in previous work, the drying efficiency increases as the mass air flow rate increases [64]. The selection of an air mass flow depends on several parameters such as the drying quality, the drying capacity and the electrical energy consumption of the ventilation. A high drying velocity can generate an exorbitant electric bill linked to the consumption of the fans and can

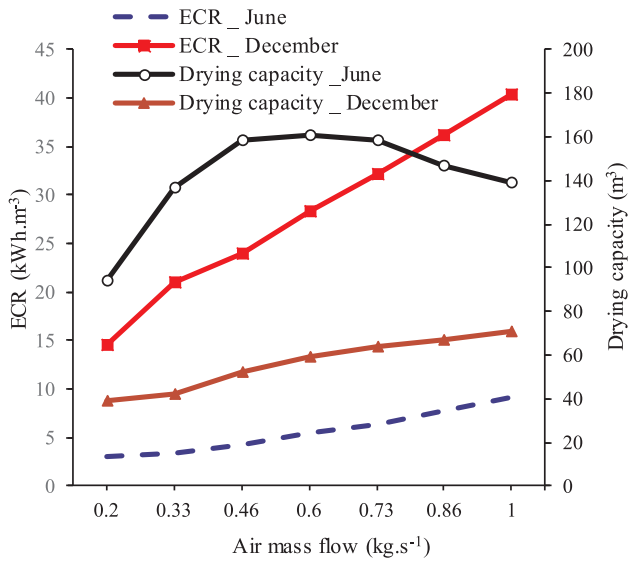

Fig. 13. Effect of air mass flow rate on drying capacity and ECR.

also affect the finish of dried products [63]. In this work, an air mass flow rate of 0.6 kg.s^{-1} is suitable in order to avoid damage and stress and thus guarantee a good quality of the dried wood.

The last section of this work is intended to conduct an in-depth study showing the effect of some parameters on softwood drying performance. Table 7 presents the influence of the set-point, the aperture area and the board size on drying performance, in June. The results show that an increase of the set temperature from 338 to 348 K leads to an increase in drying capacity from 161 to 181 m^3. There is also an increase in electricity consumption of around 42% compared to the baseline case. This increase in the set temperature has a beneficial effect on the drying efficiency which is in turn increased from 0.72 to 0.76. The results show that the decrease of the set temperature from 338 to 328 K has no significant effect on the electrical energy production and drying efficiency. However, the decrease of the set temperature from 338 to 328 K leads to reduce the electrical energy consumption by 24% and decrease the drying capacity by 10%. In a previous work, the set temperature fluctuated between 311 and 333 K by drying a stack volume of 13 m^3 using an air/air heat pump combined with electric coils [16]. The drying time was found to be 206 h and the electrical energy consumption was 1095 kWh. The results demonstrated that an increase of the aperture area from 100 to 150 m^2 has the effect of improving the electricity production and drying capacity by 45 and 27%, respectively. There is a decrease in electricity consumption of around 9% compared to the baseline drying case. In fact, as the solar collector area increases, the air temperature also increases, which reduces the drying time and consequently increases the drying cycle number [37]. In Table 7, it can be seen that a decrease of the aperture area from 100 to 50 m^2 leads to a reduction of the electrical energy production and drying capacity by about 50 and 45%, respectively. The drying efficiency also dropped from 0.72 to 0.48. The selection of an optimal aperture area depends on several parameters such as the drying time, the drying quality and the level cost of dried wood [65]. Although the drying time is reduced for a very large mirror surface, the quality of the dried products and their cost price limit this choice [66]. In this work, an aperture area of 100 m^2 is favorable for carrying out the wood drying process in good conditions. The results also show that a decrease of the board thickness from 0.025 to 0.0125 m has the effect of increasing the electrical energy consumption by 20% and improving the drying capacity by 74%. The drying efficiency fell from 0.72 to 0.93. In contrary, an increase of the board thickness from 0.025 to 0.05 m has the effect of reducing the electrical energy consumption by 16% and decreasing the drying capacity by 40%. The drying efficiency also dropped from 0.72 to 0.43.

Table 7
Effect of certain parameters on thermal drying performance in June.

		HP set –temperature « T_{set} » (K)			CPV/T mirror aperture area « S_{co} » (m^2)			Board thickness « e » (m)	
	Baseline: (T_{set} = 338 K, S_{co} = 100 m^2, e = 0.025 m	328	348		50	150		0.0125	0.05
Electrical energy production (kWh)	7098	7098	7098		3480	10,334		7098	7098
Electrical energy consumption (kWh)	881	672	1252		970	802		1058	742
Drying capacity (m^3)	161	145	181		89	205		280	97
Drying efficiency (-)	0.72	0.73	0.76		0.48	0.80		0.93	0.43

These results show that the drying capacity decreases with increasing panel thickness since the drying time increases as the board thickness increases, as reported in previous work [37,39,45,51].

5. Conclusion

In this work, a water/air heat pump powered by a concentrated photovoltaic thermal system was proposed as an innovative hybrid solution for carrying out the drying process of softwood. A mathematical model has been proposed for each component constituting the hybrid solar drying system. The perfect agreement was obtained between the experimental and numerical results. The results showed that the drying time and the energy consumption ratio decreased from January to July, then increased thereafter. The results also demonstrated that the specific moisture extraction rate and the coefficient of performance increased as the outdoor air temperature increased and the set-point decreased. In fact, a decrease of the heat pump set temperature from 75 to 65 °C improved the coefficient of performance at least 17%. Moreover, the combined use of a heat pump and a concentered photovoltaic thermal system has the effect of reducing the electrical energy consumption ratio by 39 and 86%, in January and July, respectively. The effect of some physical and geometrical parameters on thermal performance has been studied. The results showed that the drying performance decreased as the optical efficiency and the concentration factor decreased. In fact, a drop in optical efficiency from 0.9 to 0.65 has the effect of increasing the electrical energy consumption ratio by 73%. Increasing the aperture area from 100 to 150 m^2 also improved electricity production by 45%. Energy consumption ratio increased by about 43%, increasing the mass flow rate from 0.6 to 1 $kg.s^{-1}$. The results showed that the heat recovered in the regenerator increased as the temperature of air leaving the hybrid solar dryer increased. In addition, the board thickness has a significant effect on the drying capacity. In fact, the drying capacity decreased by 40%, increasing the board thickness from 0.025 to 0.05 m. The drying efficiency also dropped from 0.72 to 0.43.

The overall results have shown that the combined use of a water/air heat pump and a concentrated photovoltaic thermal system can reduce significantly the energy consumption during the wood drying process. The proposed drying strategy could also improve the thermal performance of hybrid solar dryers and make them more autonomous while producing more electricity and consuming less. The present drying model can be used to design efficient and hybrid solar dryers in order to calibrate their optimal size to encourage the wood industry to build cheaper indirect kilns. For future work in this research area, the performance of the hybrid solar dryer studied will be evaluated when it integrates a hydrogen fuel cell powered by the concentrated photovoltaic thermal system to continuously produce electricity and heat for drying purposes.

CRediT authorship contribution statement

Ahmed Khouya: Conceptualization, Data curation, Formal analysis, Investigation, Methodology, Software, Writing - original draft, Project administration, Resources, Validation, Visualization, Writing - review & editing.

Declaration of Competing Interest

The author declares that he has no competing financial interests or known personal relationships which could have seemed to influence the work reported in this document.

References

[1] A. Adhikari, O. Barbara, Minimizing environmental impacts of timber products through the production process “From Sawmill to Final Products”, Environ. Syst. Res. 7 (2018) 6, https://doi.org/10.1186/s40068-018-0109-x.
[2] A. Motevali, et al., Evaluation of energy consumption in different drying methods, Energy Convers. Manage. 52 (2011) 1192–1199, https://doi.org/10.1016/j.enconman.2010.09.014.
[3] A. Motevali, et al., Comparison of energy parameters in various dryers, Energy Convers. Manage. 87 (2014) 711–725, https://doi.org/10.1016/j.enconman.2014.07.012.
[4] G. Bhander, W. Jozewicz, Analysis of emission reduction strategies for power boilers in the US pulp and paper industry, Energy Emiss. Control Technol. 5 (2017) 27–37, https://doi.org/10.2147/EECT.S139648.
[5] K. Phonetip, et al., Drying timber in a solar kiln using an intermittent drying schedule of conventional laboratory kiln, Drying Technol. 37 (2019) 1300–1312, https://doi.org/10.1080/07373937.2018.1496337.
[6] H. Mahmudul, A.G.L. Timothy, Development of a sustainable methodology for life-cycle performance evaluation of solar dryers, Sol. Energy 135 (2016) 1–13, https://doi.org/10.1016/j.solener.2016.05.036.
[7] A.A. Chiniforush, H. Valipour, A. Akbarnezhad, Water vapor diffusivity of engineered wood: Effect of temperature and moisture content, Constr. Build. Mater. 224 (2019) 1040–1055, https://doi.org/10.1016/j.conbuildmat.2019.08.013.
[8] J.S. Tumuluru, Specific energy consumption and quality of wood pellets produced using high-moisture lodgepole pine grind in a flat die pellet mill, Chem. Eng. Res. Des. 110 (2016) 82–97, https://doi.org/10.1016/j.cherd.2016.04.007.
[9] N.M. Yacine, A. Belhamri, Effects of the climatic conditions and the shape on the drying kinetics, Application to solar drying of potato-case of Maghreb's region, J. Clean. Prod. 183 (2018) 1241–1251, https://doi.org/10.1016/j.jclepro.2018.02.103.
[10] S. Hatami, G. Payganeh, A. Mehrpanahi, Energy and exergy analysis of an indirect solar dryer based on a dynamic model, 118809, J. Clean. Prod. 244 (2020), https://doi.org/10.1016/j.jclepro.2019.118809.
[11] Q. Zhang, et al., Techno-economic analysis of air source heat pump applied for space heating in northern China, Appl. Energy 207 (2017) 533–542, https://doi.org/10.1016/j.apenergy.2017.06.083.
[12] R. Daghigh, et al., Review of solar assisted heat pump drying systems for agricultural and marine product, Renew. Sustain. Energy Rev. 14 (2010) 2564–2579, https://doi.org/10.1016/j.rser.2010.04.004.
[13] T. Kivevele, Z. Huan, A review on opportunities for the development of heat pump drying systems in South Africa, S. Afr. J. Sci. 110 (2014), https://doi.org/10.1590/sajs.2014/20130236.
[14] A. Szekeres, J. Jeswiet, Effects of hourly temperature changes and electricity generation on greenhouse gas emissions, Int. J. Energy Environ. Eng. 10 (2019) 157–179, https://doi.org/10.1007/s40095-018-0292-6.
[15] E. Mohamed, S. Riffat, S., Omer, Low-temperature solar-plate-assisted heat pump: A developed design for domestic applications in cold climate. Int. J. Refrig. 81(2017) 134-150. https://doi.org/10.1016/j.ijrefrig.2017.05.020.
[16] V. Minea, Efficient energy recovery with wood drying heat pumps, Drying Technol. 30 (2012) 1630–1643, https://doi.org/10.1080/07373937.2012.701261.
[17] B. Yuehong, et al., Performance optimization of irreversible air heat pumps considering size effect, Int. J. Therm. Sci. 27 (2018) 223–229, https://doi.org/10.1007/s11630-018-1003-6.
[18] N. Colak, A. Hepbasli, A review of heat pump drying: Part 1 – Systems, models and studies, Energy Convers. Manage. 50 (2009) 2180–2186, https://doi.org/10.1016/j.enconman.2009.04.031.
[19] A. Alishah, et al., Solar-assisted heat pump drying of coriander: an experimental investigation, Int. J. Air-Conditioning Refrigeration 26 (2018) 1850037, https://doi.org/10.1142/S2010132518500372.
[20] Z. Zhao, et al., Experimental research of a water-source heat pump water heater system, Energies 11 (2018) 1205, https://doi.org/10.3390/en11051205.
[21] L.M. López-Ochoa, et al., Solar domestic hot water regulation in the Latin American residential sector with the implementation of the Energy Performance of Buildings Directive: The case of Chile, Energy 188 (2019) 115985, https://doi.org/10.1016/j.energy.2019.115985.
[22] Z. Wang, et al., Optimal planning of a 100% renewable energy island supply system based on the integration of a concentrating solar power plant and desalination units, Int. J. Electr. Power Energy Syst. 117 (2020) 105707, https://doi.org/10.1016/j.ijepes.2019.105707.
[23] E. Psimopoulos, et al., Techno-economic analysis of control algorithms for an exhaust air heat pump system for detached houses coupled to a photovoltaic system, Appl. Energy 249 (2019) 355–367, https://doi.org/10.1016/j.apenergy.2019.04.080.
[24] J. Assafa, B. Shabanib, Experimental study of a novel hybrid solar-thermal/PV-hydrogen system: Towards 100% renewable heat and power supply to standalone applications, Energy J. 157 (2018) 862–876, https://doi.org/10.1016/j.energy.2018.05.125.
[25] D. Cocco, L. Migliari, M. Petrollese, A hybrid CSP–CPV system for improving the dispatchability of solar power plants, Energy Convers. Manage. 114 (2016) 312–323, https://doi.org/10.1016/j.enconman.2016.02.015.
[26] N. Gakkhar, S.M. Kumar, S. Jakhar, Experimental and theoretical analysis of hybrid concentrated photovoltaic/thermal system using parabolic trough collector, 115069, Appl. Therm. Eng. 171 (2020), https://doi.org/10.1016/j.applthermaleng.2020.115069.
[27] S. Ghaem Sigarchian, et al., Optimum design of a hybrid PV–CSP–LPG microgrid with Particle Swarm Optimization technique, Appl. Therm. Eng. 109(2016) 1031-1036. https://doi.org/10.1016/j.applthermaleng.2016.05.119.
[28] R. Daneshazarian, et al., Concentrating photovoltaic thermal (CPVT) collectors and systems: Theory, performance assessment and applications, Renew. Sustain. Energy Rev. 81 (2018) 473–492, https://doi.org/10.1016/j.rser.2017.08.013.

[29] W. Ben Youssef, et al., Assessment viability of a Concentrating Photovoltaic/Thermal-energy cogeneration system (CPV/T) with storage for a textile industry application, Sol. Energy. 159(2018) 841–851. https://doi.org/10.1016/j.solener.2017.11.058.
[30] F. Calise, L. Vanoli, Parabolic trough photovoltaic/thermal collectors: design and simulation model, Energies 5 (2012) 4186–4208.
[31] A. Buonomano, F. Calise, M. Dentice, L. Vanoli, A novel solar trigeneration system based on concentrating photovoltaic/thermal collectors. Part 1: design and simulation model, Energy 61(2013) 59–71. https://doi.org/10.1016/j.energy.2013.02.009.
[32] M. Proell, H. Karrer, C.J. Brabec, A. Hauera, The influence of CPC reflectors on the electrical incidence angle modifier of c-Si cells in a PVT hybrid collector, Sol. Energy 126 (2016) 220–230, https://doi.org/10.1016/j.solener.2016.01.012.
[33] M. Kandil, et al., Assessment of high concentrated photovoltaic/thermal collector in hot climate, Smart Grid and Renewable Energy 10 (2019) 119–140, https://doi.org/10.4236/sgre.2019.105008.
[34] H. Mahmudul, A.G.L. Timothy, Numerical simulation of a solar kiln design for drying timber with different geographical and climatic conditions in Australia, Drying Technol. 32 (2014) 1632–1639, https://doi.org/10.1080/07373937.2014.915556.
[35] H. Mahmudul, A.G.L. Timothy, Time-valued net energy analysis of solar kilns for wood drying: A solar thermal application, Energy J. 96 (2016) 415–426, https://doi.org/10.1016/j.energy.2015.11.081.
[36] D. Luna, J.P. Nadeau, Y. Jannot, Model and simulation of a solar kiln with energy storage, Renew. Energy 35 (2010) 2533–2542, https://doi.org/10.1016/j.renene.2010.03.024.
[37] A. Khouya, Effect of regeneration heat and energy storage on thermal drying performance in a hardwood solar kiln, Renew. Energy 155 (2020) 783–799, https://doi.org/10.1016/j.renene.2020.03.178.
[38] R. Yamsaengsung, T. Sattho, Superheated steam vacuum drying of rubberwood, Drying Technol. 26 (2008) 798–805, https://doi.org/10.1080/07373930802046518.
[39] A. Khouya, A. Draoui, Détermination des courbes caractéristiques de séchage de trois espèces de bois, Revue des Energies Renouvelables 12 (2009) 87–98.
[40] L. Haolu, et al., Design and thermal analysis of an air source heat pump dryer for food drying, Sustainability 10 (2018) 3216, https://doi.org/10.3390/su10093216.
[41] D.M. Elustondo, L. Oliveira, Model to assess energy consumption in industrial lumber kilns, Maderas. Ciencia y tecnología 11 (2009) 33–46, https://doi.org/10.4067/S0718-221X2009000100003.
[42] G. Milić, et al., Energy consumption of beech timber drying in oscillation climates, Drvna Industrija 65 (2014) 309–314, https://doi.org/10.5552/drind.2014.1367.
[43] H. Quesada-Pineda, J. Wiedenbeck, B. Bond, Analysis of electricity consumption: a study in the wood products industry, Energ. Effi. 9 (2016) 1193–1206, https://doi.org/10.1007/s12053-015-9417-4.
[44] Y. Meng, et al., Energy efficiency performance enhancement of industrial conventional wood drying kiln by adding forced ventilation and waste heat recovery system: a comparative study, Maderas, Ciencia y tecnología 21 (2019) 545–558, https://doi.org/10.4067/S0718-221X2019005000410.
[45] A. Khouya, A. Draoui, Computational drying model for solar kiln with latent heat energy storage: Case studies of thermal application, Renew. Energy 130 (2019) 796–813, https://doi.org/10.1016/j.renene.2018.06.090.
[46] L. Wang, A. Toppinen, H. Juslin, Use of wood in green building: a study of expert perspectives from the UK, J. Clean. Prod. 65 (2014) 350–361, https://doi.org/10.1016/j.jclepro.2013.08.023.
[47] W. Ben Youssef, et al., Modeling and optimization of a solar system based on concentrating photovoltaic/thermal collector. Sol Energy. 170(2018) 301–313. https://doi.org/10.1016/j.solener.2018.05.057.
[48] L. Micheli, et al., Performance, limits and economic perspectives for passive cooling of high concentrator photovoltaics, Sol Energy. Materials & Solar Cells 153 (2016) 164–178, https://doi.org/10.1016/j.solmat.2016.04.016.
[49] A. Ramos, et al., Optimisation of a high-efficiency solar-driven organic Rankine cycle for applications in the built environment, Appl. Energy 228 (2018) 755–765, https://doi.org/10.1016/j.apenergy.2018.06.059.
[50] G. Mittelman, A. Kribus, A. Dayan, A solar cooling with concentrating photovoltaic/thermal (CPVT) systems. Energy Convers. Manage. 48(2007) 2481–2490. https://doi.org/10.1016/j.enconman.2007.04.004.
[51] B. Lamrani, A. Khouya, A. Draoui, Energy and environmental analysis of an indirect hybrid solar dryer of wood using TRNSYS software, Sol. Energy 183 (2019) 132–145, https://doi.org/10.1016/j.solener.2019.03.014.
[52] B. Lamrani, A. Khouya, A. Draoui, Mathematical modeling and numerical simulation of a parabolic trough collector: A case study in thermal engineering, Therm. Sci. Eng. Prog. 8 (2018) 47–55, https://doi.org/10.1016/j.tsep.2018.07.015.
[53] S.T. Merlin, Z. André, R. Romain, R. Yann, Mathematical modelling and numerical simulation of a simple solar dryer for tropical wood using a collector, Appl. Therm. Eng. 131 (2018) 356–369, https://doi.org/10.1016/j.applthermaleng.2017.12.014.
[54] Ö. Zkizilkaya, Thermosensibilité de la demande électrique : identification de la part non linéaire par couplage d'une modélisation bottom-up et de l'approche bayésienne, Thèse de doctorat, École nationale supérieure des mines de Paris, 2014.
[55] S.N. Selvaraj, J.R. Simon, Performance analysis of a large geothermal heating and cooling system, Renew. Energy 122 (2018) 429–442, https://doi.org/10.1016/j.renene.2018.01.099.
[56] H.S.F. Awadalla, et al., Mathematical modelling and experimental verification of wood drying process, Energy Convers. Manage. 45 (2004) 197–207, https://doi.org/10.1016/S0196-8904(03)00146-8.
[57] M.M. Hassan, Y. Beliveau, Design, construction and performance prediction of integrated solar roof collectors using finite element analysis, Constr. Build. Mater. 21 (2007) 1069–1078, https://doi.org/10.1016/j.conbuildmat.2006.01.001.
[58] M.A. Hossain, K. Gottschalk, H.S. Hssan, Mathematical model for a heat pump dryer for aromatic plant, Procedia Eng. 56 (2013) 510–520, https://doi.org/10.1016/j.proeng.2013.03.154.
[59] D. Rim, S. Schiavon, W.W. Nazaroff, Energy and cost associated with ventilating office buildings in a tropical climate, e0122310, PLoS ONE 10 (2015), https://doi.org/10.1371/journal.pone.0122310.
[60] L. Shengchun, et al., Experimental investigation on drying performance of an existed enclosed fixed frequency air source heat pump drying system, Appl. Therm. Eng. 130 (2018) 735–744, https://doi.org/10.1016/j.applthermaleng.2017.11.068.
[61] K. Chapchaimoh, et al., Thermal characteristics of heat pump dryer for ginger drying, Appl. Therm. Eng. 95 (2016) 491–498, https://doi.org/10.1016/j.applthermaleng.2015.09.025.
[62] V. Minea, Overview of heat-pump–assisted drying systems, Part II: data provided vs results reported, Drying Technol. 33 (2015) 527–540, https://doi.org/10.1080/07373937.2014.952378.
[63] R.A. Ananias, et al., Energy consumption in industrial drying of radiata pine, Drying Technol. 30 (2012) 774–779, https://doi.org/10.1080/07373937.2012.663029.
[64] F. Ullah, M. Kang, Impact of air flow rate on drying of apples and performance assessment of parabolic trough solar collector, Appl. Therm. Eng. 127 (2017) 275–280, https://doi.org/10.1016/j.applthermaleng.2017.07.101.
[65] H. Brian, B.O. Espinoza, A decade of improved lumber drying technology, Curr. Forestry Rep. 2 (2016) 106–118, https://doi.org/10.1007/s40725-016-0034-z.
[66] R. Herrera-Díaz, et al., Effect of wood drying and heat modification on some physical and mechanical properties of radiata pine, Drying Technol. 36 (2018) 537–544, https://doi.org/10.1080/07373937.2017.1342094.